ChemComm
Chemical Communications

Accepted Manuscript

This article can be cited before page numbers have been issued, to do this please use: P. Gai, X. Kong, S. Zhang, P. Song and F. Li, *Chem. Commun.*, 2020, DOI: 10.1039/D0CC03039B.

ROYAL SOCIETY OF CHEMISTRY

rsc.li/chemcomm

ROYAL SOCIETY OF CHEMISTRY View Article Online
DOI: 10.1039/D0CC03039B

Journal Name

COMMUNICATION

Photo-Driven Self-Powered Biosensor for Ultrasensitive MicroRNA Detection *via* DNA Conformation-Controlled Co-Sensitization Behavior†

Received 00th January 20xx,
Accepted 00th January 20xx

DOI: 10.1039/x0xx00000x

www.rsc.org/

Panpan Gai, Xinke Kong, Shuxia Zhang, Panpan Song, and Feng Li*

We successfully developed a photoelectrochemical enzymatic fuel cell (PEFC)-based self-powered biosensing platform for microRNA detection *via* DNA conformation change-controlled co-sensitization behavior, which could offer an ultrasensitive detection of microRNA down to 0.05 fM and realize the microRNA determination in human serum.

Self-powered biosensors have been regarded as highly promising candidates for bioanalysis owing to their unique merits of working without external power source and simple instrumentation.[1-4] Currently, many self-powered biosensors were fabricated based on enzymatic fuel cells (EFCs), which has been applied in food safety,[5, 6] disease diagnosis,[7-11] environmental monitoring,[12] and so on. However, the inherently debatable issue of the anodic enzymes (widely used glucose oxidase) bioelectrocatalysis mechanism for glucose oxidation has always existed.[13] To address the above issues, photoelectrochemical enzymatic fuel cell (PEFC) could be one alternative method because of its direct photo-oxidation property and the feature of no need of anode enzyme and noble metal catalyst.[14] On this basis, some PEFC-based biosensing have exhibited the features of high sensitivity, high selectivity, and low background signal.[15-18] However, their limits of detection were both about micromolar concentrations since the relative lack of signal amplification strategy restricted the sensitivity of PEFC biosensors.

Herein, the co-sensitization between p-type and n-type photovoltaic materials has been proven as one desirable method to enhance the efficiency of charge separation and electron transfer, which is very favorable in the photoelectrochemical biosensing.[19] In the traditional method, the thickness of the active layer played a virtual role for the co-sensitization, which needed the professional technology for exactly control. Thus, to simplify the assembly of co-sensitization layer, the flexible DNA chain immobilized with n-type material was selected to precisely regulate the signal change because the DNA probe conformation would affect the distance of photovoltaic materials. MicroRNA (miRNA), a biomarker of many important diseases, is endogenous single-stranded nonprotein coding RNA consist of 20–23 nucleotides. Some methods were used for miRNA determination, such as liquid chromatography–tandem mass spectrometry,[20] electrochemistry,[21-25] chemiluminescence,[26, 27] surface-enhanced Raman scattering,[28, 29] colorimetry[30] and fluorescence[31]. Although the developed strategies have been developed to improve the detection sensitivity and flexibility, the expensive instruments and skilled operators limited the practical application. Thereby, to follow the trend of clinical application, a robust biosensing platform without any external power source and simple instrumentation is in desperate need.

In our work, taking the above considerations into account, with the miRNA-141 as a model, we proposed a PEFC-based self-powered biosensor for miRNAs ultrasensitive detection based on the DNA configurational-controlled co-sensitization amplification strategy, in which, the photovoltaic materials CdS quantum dots (QDs) were ingeniously modified on the hairpin DNA probe. To design DNA conformation-controlled co-sensitization signal amplification strategy, the light-harvesting material AuNPs-g-C_3N_4 generated hole-electron pair and the electron donor glucose molecular in the supporting electrolyte solution consumed the holes to enhance the separation efficiency of hole-electron. Upon illumination, in the absence of target miRNA, the conformation of DNA probe was in the hairpin form, thus the bounded CdS-COOH QDs were close to AuNPs-g-C_3N_4, which resulted in a high photocurrent response because the formed co-sensitized structure could further promote the separation efficiency of hole-electron pair. In this case, the generated electrons transferred to the

College of Chemistry and Pharmaceutical Sciences, Qingdao Agricultural University, Qingdao 266109, P. R. China.

*Corresponding author. Tel/Fax: 86-532-58957855 E-mail: lifeng@qau.edu.cn

†Electronic Supplementary Information (ESI) available: [Experimental section, Gel electrophoresis, Photocurrent responses, the absorbance and photoluminescence spectra of the photoanode; TEM image of AuNPs; CVs of the G/CNTs/AuNPs modified ITO electrode; EIS of the biocathode electrode; sequences of the oligonucleotides used in the experiments; comparison of analytical performance for miRNA assay; measurement of the serum samples]. See DOI: 10.1039/x0xx00000x

View Article Online
DOI: 10.1039/D0CC03038F

graphene/carbon nanotubes/gold nanoparticles/laccase (G/CNTs/AuNPs/laccase) biocathode and realized the O_2 reduction, producing a higher E^{OCV}. However, once the target miRNA was captured, the hairpin DNA probe would hybridize with the target to form a more rigid, rodlike double helix, which drove the anchored CdS-COOH QDs away from the AuNPs-g-C_3N_4 electrode surface. Therefore, the photocurrent responses significantly decreased owing to the vanished sensitization effect, thereby producing a lower E^{OCV} of the PEFC. Consequently, the proposed bioassay for ultrasensitive detection of miRNA was readily realized according to the E^{OCV} variation. This work provides an idea for designing the new types of self-powered biosensing platform *via* DNA conformation-controlled signal amplification strategy.

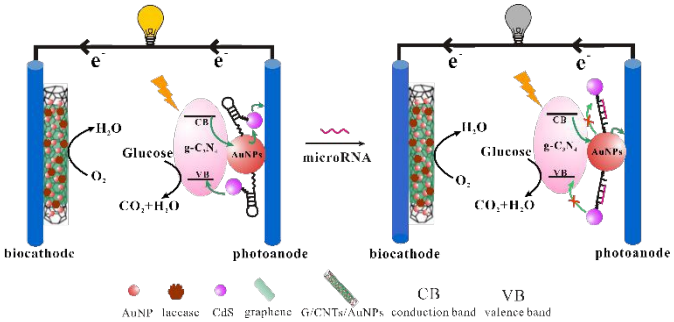

Scheme 1. Schematic Illustration of the Principle of the PEFC-Based Self-Powered Biosensing platform.

For the photoanode, the assembly process was shown in Fig. 1A. The hairpin DNA probe was immobilized on the AuNPs-g-C_3N_4 surface *via* the Au-S bond. Subsequently, 6-mercapto-1-hexanol (MCH) was coated on the surface of the electrode to block the non-specific active sites. Afterwards, the signal amplification elements CdS-COOH QDs were labeled on the terminal of hairpin DNA probe through condensation reaction. Once the target miRNA was present, the hairpin DNA probe would hybridize with the target to form a more rigid, rodlike double helix, which drove the anchored CdS-COOH QDs away from the AuNPs-g-C_3N_4 electrode surface. The light harvesting material AuNPs-g-C_3N_4 was selected not only because its advantages of low toxicity, high chemical stability, inexpensive precursors, and the simple preparation process.[32, 33]but also that AuNPs were utilized to improve the photocurrent because of the surface plasmons polaritons effect.[34] The morphology of the g-C_3N_4 and AuNPs-g-C_3N_4 was characterized by TEM. As shown in Fig. 1B, the pristine g-C_3N_4 film clearly presented a wrinkled structure. While the AuNPs-g-C_3N_4 showed that lots of AuNPs (little dark spots) adhered to the g-C_3N_4 surface (Fig. 1C), indicating the successful preparation of AuNPs-g-C_3N_4. In addition, EIS (Fig. 1D) was carried out with $[Fe(CN)_6]^{3-/4-}$ as the redox probe to verify the modification process in Fig.1A. The charge-transfer resistance (R_{ct}) value of the bare ITO was small (90.8 Ω, curve b), while the R_{ct} value of AuNPs-g-C_3N_4 /ITO electrode (72.4 Ω, curve a) exhibited a slightly decreased, which might attributed to the fact that the enlarge effective surface area of the AuNPs-g-C_3N_4 electrode could facilitate the redox probe diffusion to electrode surface. Nevertheless, the introduction of hairpin DNA made the R_{ct} value increased (101.8 Ω, curve c), owing to the large steric hindrance and the poor electrical conductivity of DNA. Subsequently, the R_{ct} value further increased (140.6 Ω, curve d) after the modification of CdS QDs, which could be explained that the adsorption of semiconductor CdS QDs with poor electrical conductivity blocked the electron transfer from ferricyanide to the electrode. The conjugation reaction between the NH_2-DNA and CdS QDs was also confirmed by the gel electrophoresis (The detailed experiment and Fig. S1 were shown in ESI†). When miRNA was captured by the above electrode, the R_{ct} value continued to increase (187.8 Ω, curve e), owing to the big steric hindrance of DNA and the electrostatic repulsion between the negatively charged DNA, CdS QDs and the redox probe. The obtained results strongly demonstrated the successful assembly of the ITO/AuNPs-g-C_3N_4/HS-DNA-NH_2/ CdS/miRNA photoanode.

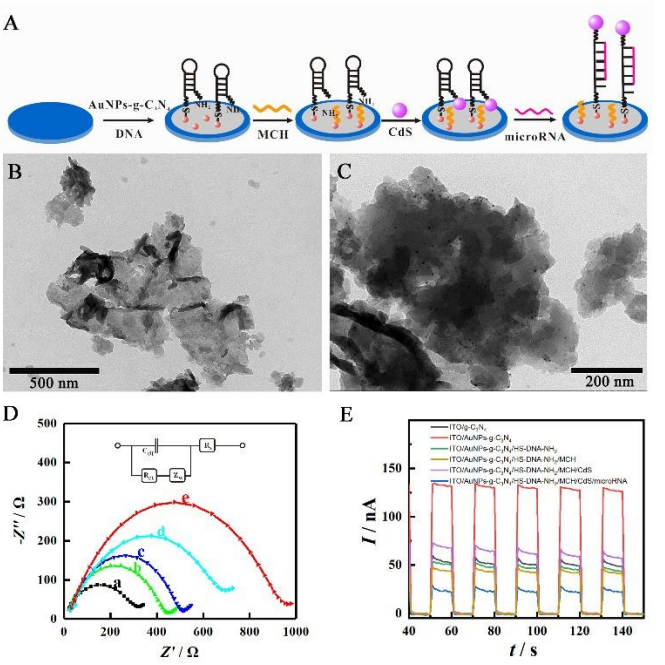

Fig. 1. (A) Assembly process of the ITO/AuNPs-*g*-C_3N_4/HS-DNA-NH_2/MCH/CdS/miRNA photoanode. TEM images of (B) g-C_3N_4 and (C) AuNPs-g-C_3N_4. (D) EIS curves of the different electrodes: (a) the ITO/AuNPs-g-C_3N_4, (b) the bare ITO electrode, (c) the ITO/AuNPs-g-C_3N_4/HS-DNA-NH_2, (d) the ITO/AuNPs-g-C_3N_4/HS-DNA-NH_2/MCH/CdS, (e) the ITO/AuNPs-g-C_3N_4/HS-DNA-NH_2/MCH/CdS/miRNA. (E) Photocurrent responses of the photoanode in 0.1 M pH 7.4 PB containing 0.1M glucose at 0 V with light excitation.

Furthermore, we also investigated the photocurrent change during the above assembly process to check the feasibility of biosensing. As illustrated in Fig. 1E, compared to neat *g*-C_3N_4 modified ITO electrode (curve c), a strong photocurrent response was produced for the AuNPs-g-C_3N_4/ITO electrode (curve a), which could be ascribed to the surface plasmons polaritons effect of metal nanoparticles. Subsequently, as the hairpin DNA probe was immobilized on the AuNPs-g-C_3N_4 electrode, the photocurrent intensity obviously decreased (curve e). However, after the CdS QDs anchored, the photocurrent response significantly increased (curve b), which could be attribute to the co-sensitization CdS QDs enhanced the separation efficiency of hole-electron pair. Once the target

miRNA-141 existed (curve f), the hairpin DNA probe could hybridize with miRNA to form a more rigid, rod-like double helix, driving the CdS QDs away from the AuNPs-g-C_3N_4. In this case, the heterojunction structure was destroyed, leading to the reduction of the electron-hole pair separation efficiency. It should be noted that the photocurrent response signal gradually decreased with the increase of miRNA concentration (Fig. S2, ESI†). To further confirm the mechanism of electron-hole pair separation efficiency for AuNPs-g-C_3N_4/CdS, the absorption and photoluminescence spectra were performed. The g-C_3N_4 showed a certain absorption at 430 nm, and the AuNPs-g-C_3N_4/CdS hybrid could address the inherent weak absorption defect of g-C_3N_4 (Fig. S3A, ESI†), thus 430 nm was selected as light illumination for PEC measurement. Fig. S 3B in ESI† showed that AuNPs could quench the photoluminescence of g-C_3N_4, and compared to AuNPs quenching the photoluminescence of g-C_3N_4, AuNPs-g-C_3N_4/CdS showed a more obvious photoluminescence quenching. Furthermore, in the presence of 1pM miRNA, the photoluminescence of AuNPs-g-C_3N_4/CdS/miRNA almost recovered to initial value, which perfectly explained the above electrochemical characterization and indicated the existence of CdS significantly promoted the electron-hole pair separation efficiency in AuNPs-g-C_3N_4. The as-proposed target-induced signal response laid a solid foundation for miRNA selective detection and quantification.

In the PEFC-based self-power biosensor, the biocathode also played an important role. Herein, the G/CNTs/AuNPs was selected as the substrate material to bound laccase via the condensation reaction between the carboxyl groups on the Au NPs and the amino groups in enzyme structure. Firstly, TEM was used to characterize the morphology of the obtained G/CNTs/AuNPs. The AuNPs exhibited a uniform diameter of ~10 nm (Fig. S4, ESI†) and distributed on the surface of G/CNTs composites Fig. 2A, suggesting the successful preparation of G/CNTs/AuNPs substrate material.

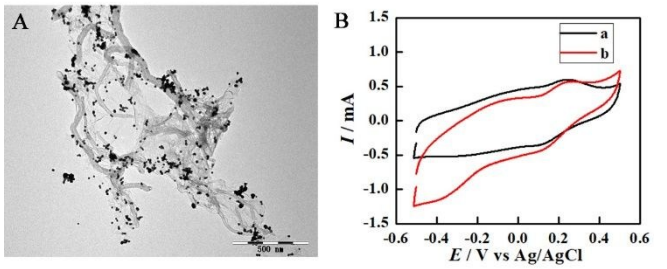

Fig. 2. (A) TEM image of G/CNTs/AuNPs. (B) CV curves of the G/CNTs/AuNPs/laccase biocathode in PB (pH = 7.4) saturated with N_2 (a) and O_2 (b) with the scan rate of 50 mV s^{-1}.

In this case, the biocatalysis properties of the biocathode was studied by the CVs measurement. Firstly, the deletional control experiments were carried out in which the laccase was removed. For the substrate materials G/CNTs/AuNPs, CVs curves were no obvious change regardless of the presence of oxygen (Fig. S5, ESI†), indicating the necessity of the cathodic enzyme. For the G/CNTs/AuNPs/laccase biocathode, an obvious reduction current was observed in the presence of O_2 compared with that of N_2 (Fig. 2B), indicating that the as-prepared biocathode possessed good bioelectrocatalytic ability for O_2 reduction. The above results from the as-prepared photoanode and biocathode ensured the construction of the photo-driven self-powered biosensing platform for miRNA assay.

The PEFC-based self-powered biosensor was fabricated for the miRNA determination via integration of the ITO/AuNPs-g-C_3N_4/DNA/CdS photoanode and the ITO/G/CNTs/AuNPs/laccase biocathode, the E^{OCV} of which could reach 0.62 ± 0.01 V. The responses of the as-constructed biosensor were measured under different concentrations of miRNA. Fig. 3A shows that the relationship between E^{OCV} and miRNA concentration exhibited a negative correlation, in which the linear relationship was well fitted between E^{OCV} and the logarithm of miRNA concentration in the range from 0.05 to 1000 fM. The linear equation was E^{OCV} = 0.5685 - 0.022log$c$ with the coefficient of determination (R^2) of 0.996. The direct detection limit was 0.05 fM. Furthermore, our biosensor showed a relatively lower detection limit for miRNA determination in the published literatures (Table S2), mainly being attributed to the design of DNA conformation-controlled co-sensitization signal amplification strategy. Although the detection limit of the as-proposed biosensor is not the lowest, the simple instrumentation and no needing external power sources in the procedure facilitated the practical application in biomedical fields.

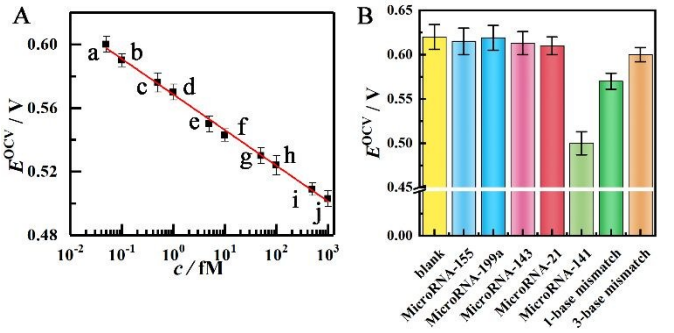

Fig. 3 (A) The relationship between the E^{OCV} and the logarithm of the miRNA concentration in 0.1 M PB solution (PH 7.4) containing 0.1 M glucose (a-j) 50.0 aM, 100.0 aM, 500.0 aM, 1.0 fM, 5.0 fM, 10.0 fM, 50.0 fM, 100.0 fM, 500.0 fM and 1.0 pM at 0 V with light excitation. (B) Selectivity analysis for miRNA detection by monitoring the E^{OCV} with 1.0 pM of interferences and 1.0 pM miRNA-141.

To verify the specificity of the as-proposed biosensor, a series of control experiments were performed to evaluate the influences of analogy miRNA such as microRNA-155, miRNA-199a, miRNA-143, miRNA-21, and the base mismatched strands as the interferences. As shown in Fig. 3B, compared to four other miRNAs, only miRNA-141 presented a relatively low E^{OCV}, attributing to its specific hybridization with hairpin DNA. In contrast, other four miRNA could not hybridization with hairpin DNA (gel electrophoresis demonstration in Fig. S1, ESI†), and the co-sensitization effect still existed, which guaranteed almost constant E^{OCV}. In addition, even one and three-base mismatched strands could not destruct the co-sensitization structure, and it exhibited the excellent selectivity of the as-proposed biosensor for miRNA-141. To investigate the stability

of the as-proposed biosensor, six biosensors were independently constructed. It was found that the E^{OCV} value barely changed after storage at 4 °C for 10 days. When the as-prepared biosensor was stored for 20 days, the E^{OCV} value still retained 89.5% of the initial responses to 10 fM miRNA-141, which demonstrated that the PEFC-based biosensor possessed good stability due to no electron mediator and bioanodic enzyme for bioassay. The excellent specificity and stability could be one important prerequisite for the as-proposed self-powered biosensors with great potential applications in accurate early-diagnosis of cancers.

On the basis of the excellent features, the diluted serum (10%) samples were measured by standard addition method to evaluate the compatibility and practicability of the sensing platform. MiRNA-141 with four different concentrations were added into human serum. As displayed in Table S3, the recoveries of 93.0%-108.0% and the RSD less than 5% were obtained, indicating that the as-proposed biosensor has great potential as an alternative candidate in real biological samples for the accurate early-diagnosis of cancers.

Conclusions

In summary, we proposed a new PEFC self-powered biosensing platform for ultrasensitive miRNA assay via AuNPs-g-C_3N_4 and CdS QDs co-sensitization strategy in the anode. In particular, CdS QDs was immobilized on the flexible DNA probe, and in this case, the DNA conformation switching from the hairpin to the rigid and rodlike double helix structure would affect co-sensitization behavior, leading to different photocurrent responses. More importantly, the proposed assay could offer an ultrasensitive detection, and the direct detection limit was 0.05 fM. Overall, the as-proposed strategy not only offered an ingenious idea for amplification to design new types of PEFC self-powered biosensing platform but also have great potential for practical application in biomedical research and clinical diagnosis.

We gratefully appreciate the financial support from the National Natural Science Foundation of China (21605092 and 21775082), the Natural Science Foundation of Shandong Province (ZR2019YQ23), Shandong Province Higher Educational Program for Young Innovation Talents, Major Program of Shandong Province Natural Science Foundation (ZR2018ZC0127), the Research Foundation for Distinguished Scholars of Qingdao Agricultural University (663-1117002) and the Special Foundation for Taishan Scholar of Shandong Province (No. ts201511052)

Conflicts of interest

There are no conflicts of interest to declare.

Notes and references

1 M. Grattieri and S. D. Minteer, *ACS Sens*, 2018, **3**, 44-53.
2 Y. Chen, W. Ji, K. Yan, J. Gao and J. Zhang, *Nano Energy*, 2019, **61**, 173-193.
3 L. Fu, J. Liu, Z. Hu and M. Zhou, *Electroanalysis*, 2018, **30**, 2535-2550.
4 M. Zhou, *Electroanalysis*, 2015, **27**, 1786-1810.
5 P. P. Gai, C. C. Gu, T. Hou and F. Li, *Anal. Chem.*, 2017, **89**, 2163-2169.
6 C. C. Gu, P. P. Gai, T. Hou, H. Y. Li, C. H. Xue and F. Li, *ACS Appl. Mater. Interfaces*, 2017, **9**, 35721-35728.
7 P. P. Gai, C. C. Gu, T. Hou and F. Li, *ACS Appl. Mater. Interfaces*, 2018, **10**, 9325-9331.
8 P. P. Gai, Y. S. Ji, W. J. Wang, R. B. Song, C. Zhu, Y. Chen, J. R. Zhang and J. J. Zhu, *Nano Energy*, 2016, **19**, 541-549.
9 C. C. Gu, P. P. Gai, L. Han, W. Yu, Q. Y. Liu and F. Li, *Chem. Commun.*, 2018, **54**, 5438-5441.
10 Y. Wang, L. Ge, P. Wang, M. Yan, J. Yu and S. Ge, *Chem. Commun.*, 2014, **50**, 1947-1949.
11 M. Zhou, N. Zhou, F. Kuralay, J. R. Windmiller, S. Parkhomovsky, G. Valdés‐Ramírez, E. Katz and J. Wang, *Angew. Chem. Int. Ed.*, 2012, **51**, 2686-2689.
12 D. Wen, L. Deng, S. Guo and S. Dong, *Anal. Chem.*, 2011, **83**, 3968-3972.
13 P. N. Bartlett and F. A. Al-Lolage, *J. Electroanal. Chem.*, 2017, **819**, 26-37.
14 Y. Yan, J. Fang, Z. Yang, J. Qiao, Z. Wang, Q. Yu and K. Sun, *Chem. Commun.*, 2013, **49**, 8632-8634.
15 L. He, Q. Liu, S. Zhang, X. Zhang, C. Gong, H. Shu, G. Wang, H. Liu, S. Wen and B. Zhang, *Electrochem. Commun.*, 2018, **94**, 18-22.
16 K. Zhao, X. Yan, Y. Gu, Z. Kang, Z. Bai, S. Cao, Y. Liu, X. Zhang and Y. Zhang, *Small*, 2015, 1502042.
17 Z. Kang, Y. Gu, X. Yan, Z. Bai, Y. Liu, S. Liu, X. Zhang, Z. Zhang, X. Zhang and Y. Zhang, *Biosens. Bioelectron.*, 2015, **64**, 499-504.
18 W.-X. Dai, L. Zhang, W.-W. Zhao, X.-D. Yu, J.-J. Xu and H.-Y. Chen, *Anal. Chem.*, 2017, **89**, 8070-8078.
19 J. Low, J. Yu, M. Jaroniec, S. Wageh and A. A. Al-Ghamdi, *Adv. Mater.*, 2017, **29**, 1601694.
20 Y. Kuang, J. Cao, F. Xu and Y. Chen, *Anal. Chem.*, 2019, **91**, 8820-8826.
21 B. Bo, T. Zhang, Y. Jiang, H. Cui and P. Miao, *Anal. Chem.*, 2018, **90**, 2395-2400.
22 J. Xu, C. Yan, X. Wang, B. Yao, J. Lu, G. Liu and W. Chen, *Anal. Chem.*, 2019, **91**, 9747-9753.
23 P. Miao, T. Zhang, J. Xu and Y. Tang, *Anal. Chem.*, 2018, **90**, 11154-11160.
24 P. P. Gai, C. C. Gu, H. Y. Li, X. Z. Sun and F. Li, *Anal. Chem.*, 2017, **89**, 12293-12298.
25 J. F. Chang, X. Wang, J. Wang, H. Y. Li and F. Li, *Anal. Chem.*, 2019, **91**, 3604-3610.
26 Y. Wang, Z. Li, Q. Lin, Y. Wei, J. Wang, Y. Li, R. Yang and Q. Yuan, *ACS Sens.*, 2019, **4**, 2124-2130.
27 Y. Sun, L. Shi, Q. Wang, L. Mi and T. Li, *Anal. Chem.*, 2019, **91**, 3652-3658.
28 Y. Sun and T. Li, *Anal. Chem.*, 2018, **90**, 11614-11621.
29 P. Strobbia, Y. Ran, B. M. Crawford, V. Cupil-Garcia, R. Zentella, H.-N. Wang, T.-P. Sun and T. Vo-Dinh, *Anal. Chem.*, 2019, **91**, 6345-6352.
30 X. Liu, H. Zhang, S. Qin, Q. Wang, X. Yang and K. Wang, *Biosens. Bioelectron.*, 2019, **129**, 87-92.
31 C. Li, C. Xue, J. Wang, M. Luo, Z. Shen and Z.-S. Wu, *Anal. Chem.*, 2019, **91**, 11529-11536.
32 T.-N. Ye, L.-B. Lv, X.-H. Li, M. Xu and J.-S. Chen, *Angew. Chem. Int. Ed.*, 2014, **53**, 6905-6909.
33 T. Y. Ma, S. Dai, M. Jaroniec and S. Z. Qiao, *Angew. Chem. Int. Ed.*, 2014, **53**, 7281-7285.
34 S. Patnaik, S. Martha, G. Madras and K. Parida, *Phys. Chem. Chem. Phys.*, 2016, **18**, 28502-28514.